

Article

# Synthesis of Core-Shell MgO Alloy Nanoparticles for Steelmaking

Jinglong Qu <sup>1</sup>, Shufeng Yang <sup>2,3,\*</sup>, Hao Guo <sup>2,3</sup>, Jingshe Li <sup>2,3</sup> and Tiantian Wang <sup>2,3</sup><sup>1</sup> Central Iron and Steel Research Institute, Beijing 100081, China; 13810256459@139.com<sup>2</sup> School of Metallurgical and Ecological Engineering, University of Science and Technology Beijing, Beijing 100083, China; guohaoustb@sina.com (H.G.); lijingshe@ustb.edu.cn (J.L.); wangtiantian@xs.ustb.edu.cn (T.W.)<sup>3</sup> Beijing Key Laboratory of Special Melting and Preparation of High-End Metal Materials, Beijing 100083, China

\* Correspondence: yangshufeng@ustb.edu.cn

Received: 4 April 2018; Accepted: 23 April 2018; Published: 27 April 2018



**Abstract:** In this present study, we aimed to reduce the wetting angle of nanoparticles (NPs) in molten steel and thus, increase their utilization ratio in steel. In order to achieve this, a two-step process was used to synthesize a core-shell AlTi-MgO@C NP structure for steelmaking through a dopamine polymerization process, which used an ammonium persulfate oxidant and high-temperature carbonization. The NP surface characterization was tested by scanning electron microscopy and field emission transmission electron microscopy, while the hydrodynamic NP size was measured by dynamic light scattering. The results showed that a carbon coating that had a thickness of 10 nm covered the NP surface, with the dispersion and stability of the particles in the aqueous solution having improved after the coating. The contact angle of the surface-treated NP was less than that of the uncoated NP in high-temperature molten steel and the corresponding wetting energy was smaller, which indicated improved wettability.

**Keywords:** MgO nanoparticle; dopamine polymerization; carbonization process; core shell structure; contact angle

## 1. Introduction

The surface modification of materials plays a vital role in modern chemistry, biology and the science of materials science. This has been widely applied in the fields of science, engineering and technology [1,2]. There are numerous and varied methods for modification, including Langmuir–Blodgett deposition, monolayer self-assembly and layer-by-layer self-assembly. This can be chosen according to optimal compatibility with the specific material requirements [3–6]. However, these methods lack efficacy on a broad range of material surfaces.

In the science of surface coatings, carbon coating technology has been widely used due to its chemical stability. Glucose has been used as a carbon source, but its specific capacity is limited due to a relatively high carbon content. Oleic acid [7], citric acid [8], ethylenediaminetetraacetic acid [9] and other organic compounds have been used as a substitute for glucose to provide a carbon source but obtaining a relatively uniform carbon layer remains a challenge.

Dopamine can be utilized to form polydopamine (PDA) in alkaline pH conditions to create oxide-induced self-polymerization [10]. After this, the PDA can become adhered to the surface of a solid material through an amino- or mercapto-nucleophilic reaction. This widely-used method exhibits strong adhesion properties, easily produces a functional modification of the material surface and is unaffected by the size and shape of the material. The advantages of dopamine-encapsulated

materials are linked to the simple reaction conditions and the homogeneous coating [11]. In addition, the thickness of the dopamine layer can be controlled by changing the initial concentration and polymerization time of the dopamine. This is important especially considering that thickness control is very important for material design and surface modification [12]. Due to the excellent and versatile coating capabilities of dopamine, it can be used as a precursor of carbon to form a uniform and continuous coating on the NP surface [13,14]. After this, by controlling the heat treatment atmosphere, the coating of PDA on the material can be converted into a carbon layer through high-temperature carbonization [15].

The purity of molten steel plays an important role in determining the properties of the steel and the distribution of second-phase nanoparticle (NP) dispersions in the steel can be used as an external method to improve steel purity [16]. This is accomplished because NPs can alter inclusion characteristics so that the precipitation of molten steel in the cooling process becomes finer and can reach sizes on even the nanoscale, avoiding the adverse effects of large inclusions in the steel [17]. However, due to the large surface properties of the NPs, they easily agglomerate in the high-temperature steel and reduce the yield.

Using these dispersant and nanoscale materials, some groups have mechanically hot-pressed the NPs mixed with the metal alloy powder in experiments, with some having added the NPs to the molten steel. The addition of the NPs was found to have a significant effect [18,19], although the NPs that entered into the welding pool were found to gather and float to the surface of the steel liquid. Thus, the second-phase particle yield in oxide metallurgy technology is a key problem that must be solved before this production can be applied for real-life applications [20]. In this study, NP surfaces were modified by a chemical method. The characterization showed that the treated NPs had good stability and dispersibility, with successful preparation of NPs with a core-shell structure. The surface coating method was beneficial in reducing the contact angle between the NP and the steel liquid and in improving the yield of the nanoparticles in the steel liquid.

## 2. Materials and Methods

### 2.1. Materials

The dopamine hydrochloride and ammonium persulfate used in this present study were purchased from Sigma (Beijing, China), while the Al, Ti and MgO NPs were purchased from Chao Wei Co., Ltd. (Shanghai, China). All other chemicals used were of at least analytical reagent grade and were obtained from Sinopharm Chemical Reagent Co., Ltd. (Beijing, China). Aqueous solutions were prepared using deionized water (Milli-Q system).

Our first aim was to improve the dispersion of the MgO NPs in liquid steel. Firstly, the AlTi (diameter of 50–70 nm) NP alloy was manufactured by mechanically mixing the individual NPs with a weight ratio of Al and Ti NP of 7:3. This NP mixture was called the AlTi alloy NP. The AlTi (Al with 70 wt %; Ti with 30 wt %) NP alloy and the MgO NPs were mixed in a planetary ball mill (IKN Mechanical Equipment Co., Ltd., Berlin, Germany) with a mass fraction of the MgO to AlTi alloy of 5:1. During mixing, the planetary ball mill was operated at 6500 rpm/min for 4 h at a low temperature and under low oxygen conditions, which aims to avoid the risk of high temperatures resulting from particle collisions.

### 2.2. Characterization

The morphologies and chemical compositions of the samples were measured using field emission scanning electron microscopy (SEM, Hitachi, Tokyo, Japan) and field emission transmission electron microscopy (TEM, Hitachi, Tokyo, Japan). X-ray diffraction spectra (XRD, PANalytical Co., Ltd., Amsterdam, The Netherlands) of the samples were obtained at a scan rate of 1°/min. The hydrodynamic sizes of NPs were measured by dynamic light scattering (DLS, Malvern, Worcestershire, UK) in deionized water at room temperature.

### 2.3. Preparation of AlTi-MgO@PDA nanoparticles (NPs)

To coat the NPs with PDA, 300 mg of dopamine hydrochloride and 300 mg of AlTi-MgO NPs were added to a phosphate-buffered solution (0.1 M, pH of 7.0) with magnetic stirring for 2 h. After this, 170 mg of ammonium persulfate was added into the mixture, which was stirred for another 1 h. This produced AlTi-MgO@PDA NPs, which were obtained after several rounds of centrifugation and washing with distilled water and ethanol. All reactions were conducted at room temperature. The process of self-polymerization is shown in Figure 1.

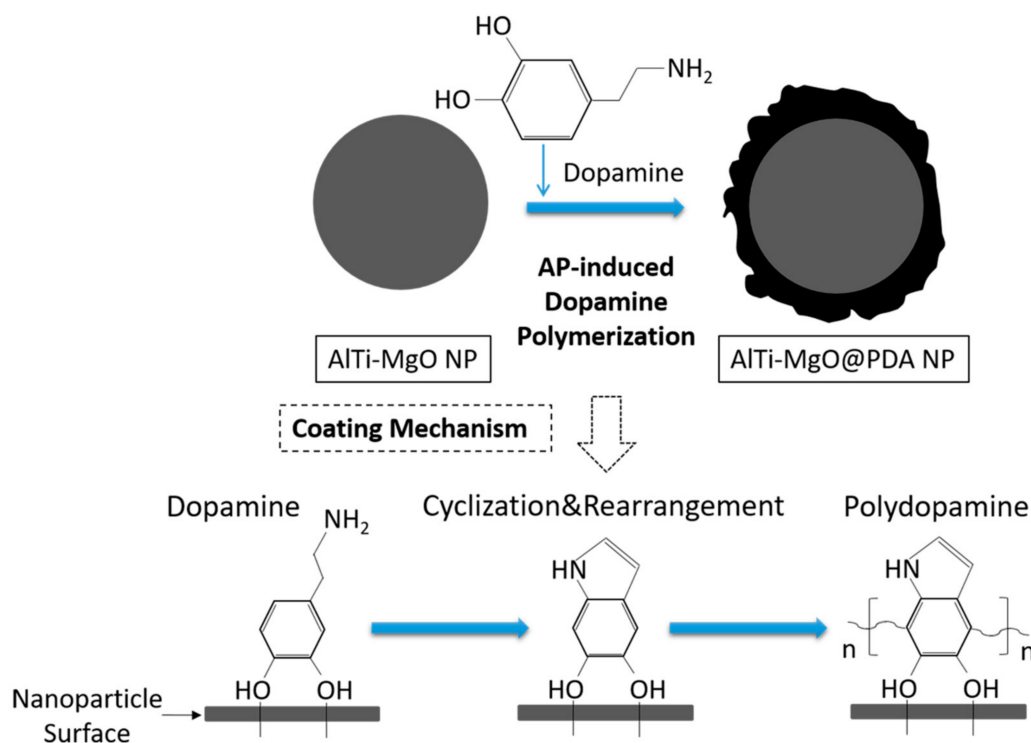


**Figure 1.** Schematic diagram of the formation of the PDA film on AlTi-MgO nanoparticles (NPs).

### 2.4. Preparation of AlTi-MgO@C NPs

To carbonize the PDA film, the AlTi-MgO@PDA NPs were placed into a tubular furnace, which was maintained at 550 °C for 4 h in a nitrogen environment. After the heat treatment, the AlTi-MgO@C NPs were soaked in a 0.24 M HCl solution for 30 min, before being rinsed several times with deionized water. Figure 2 shows the process of the high-temperature carbonization of NPs.

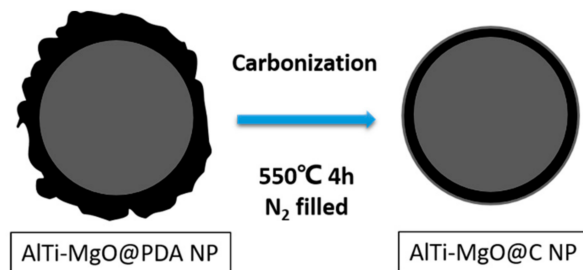


**Figure 2.** Schematic diagram of the formation of the carbon film after heat treatment.

### 3. Results

#### 3.1. NP Characteristics

Figure 3 shows the typical SEM and TEM images of the AlTi-MgO NP cores for steelmaking. After the pre-dispersion ball-milling treatment, the NPs were shown to be spherical with a smooth surface that exhibits no coating. Figure 3C shows the XRD pattern of the AlTi-MgO NPs, which depicts many narrow peaks. The narrowness of the peaks indicated that the NPs have good crystallinity after the pre-dispersion treatment. The corresponding phases were identified as Al and Ti as individual substances and MgO oxide. Furthermore, the MgO NPs easily combined with the water vapor in the air to form Mg(OH)<sub>2</sub>.

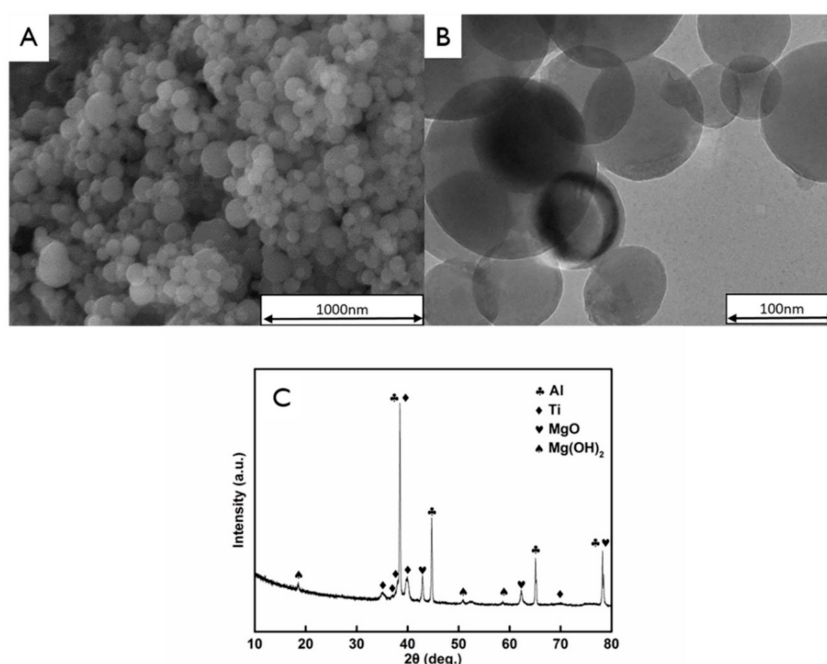
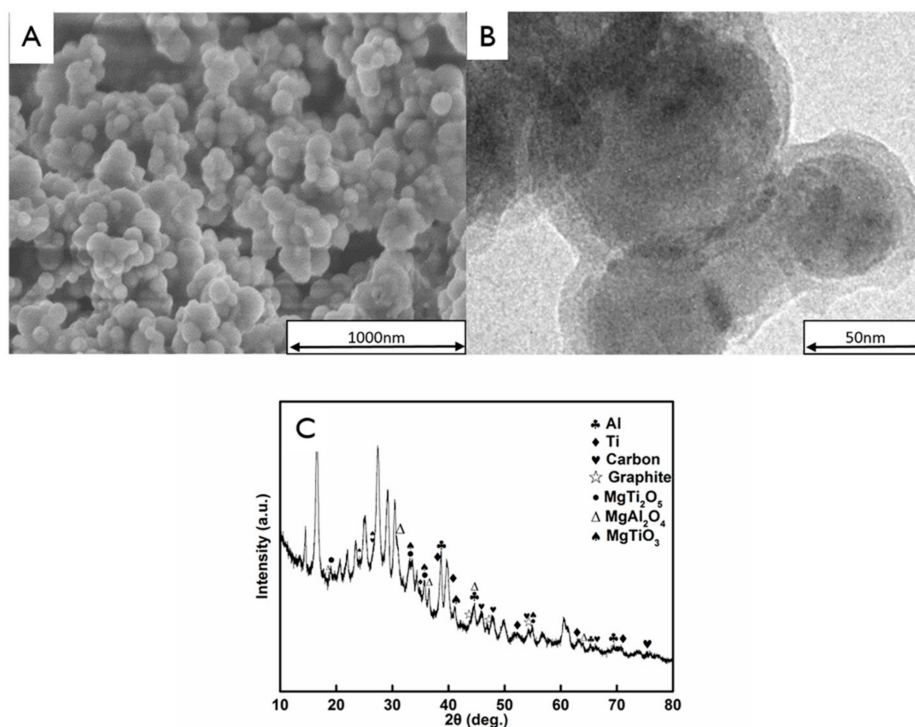


**Figure 3.** Analysis of the bare AlTi-MgO NPs, showing the: (A) Scanning electron microscopy (SEM) image; (B) Transmission electron microscopy (TEM) image; and (C) X-ray diffraction spectra (XRD) pattern.

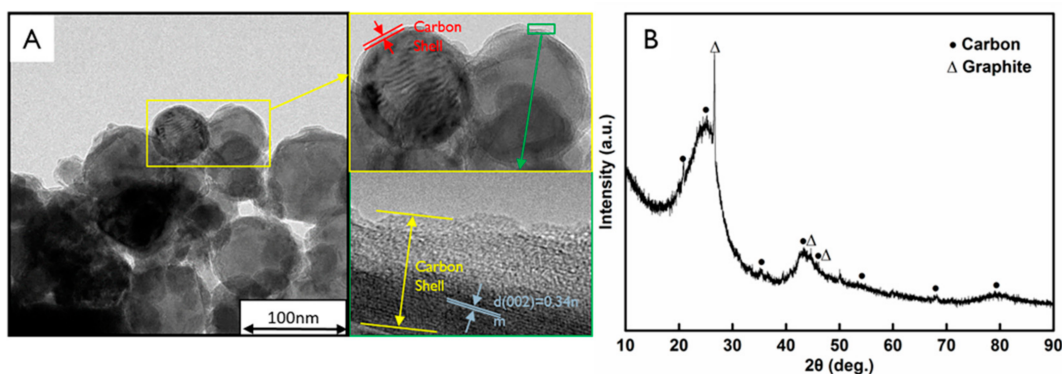
Figure 4 shows the typical SEM and TEM images of the AlTi-MgO@PDA NPs for steelmaking. The SEM image (Figure 4A) shows that after the process of dopamine self-polymerization induced by the ammonium persulfate oxidant, the surface of the NP becomes rough, which is the typical morphology of a dopamine self-polymerization covering. The shell layer of these surface-treated NPs had a thickness of approximately 7–18 nm, which was measured from the comparison of the TEM images with the original NP diameters (Figure 3B). Figure 4C shows the XRD pattern of the AlTi-MgO@PDA NPs. After heating at 550 °C for 4 h in a nitrogen environment, a proportion of the Al and Ti was retained as individual substances and the mass fraction of the MgO NPs was relatively small. The corresponding metal complex oxide phases with Al and Ti elements were easily formed at this high temperature: MgTiO<sub>3</sub>, MgTi<sub>2</sub>O<sub>5</sub> and MgAl<sub>2</sub>O<sub>4</sub> phases. At the same time, the amorphous carbon and graphitic carbon phases appeared with a broadened peak, which indicated that a C-AlTi-MgO composite phase was formed after the carbonization process.

Figure 5 shows the TEM images of AlTi-MgO@C NPs after the carbonization process. During this process, the structure of the surface organic substance breaks down and the loss of these hybrid atoms leads to a contraction of the PDA film [21]. The high-resolution TEM images are shown in Figure 5A (insets), which demonstrated that the outer layer of the particle is coated with a carbon

layer. No obvious lattice fringes can be observed in the outer layer of the carbon shell, while the inner layer of the coating exhibits an inter-crystalline spacing of  $d_{(002)} = 0.34$  nm, which corresponds to the graphitic carbon crystal. After dispersion and carbonization, no obvious agglomeration phenomenon was observed and the particles were well dispersed in the aqueous solution. Figure 5B shows the XRD pattern of the AlTi-MgO@C NPs after hot HCl acid pickling for 30 min, which exhibits peak shapes that corresponded to amorphous carbon and graphite. Furthermore, the latter peak showed good crystallinity. According to these results, AlTi-MgO@C NP were synthesized after the surface treatment.



**Figure 4.** Analysis of the AlTi-MgO NPs coated with PDA, showing the: (A) SEM image; (B) TEM image; and (C) XRD pattern.



**Figure 5.** (A) High-resolution TEM images of the AlTi-MgO@C NP and (B) XRD pattern of the AlTi-MgO NP after HCl acid pickling for 30 min.

Figure 6 shows the size distribution of the AlTi-MgO, AlTi-MgO@PDA core-shell and AlTi-MgO@C core-shell NP samples. The dynamic light scattering (DLS) measurement detected one particle size in each aqueous solution. The average size of the AlTi-MgO NPs was approximately 50 nm, while the AlTi-MgO@PDA NP size increased to 70 nm after the surface modification. This reflects

a combination of the core diameter (50 nm) and the shell (20 nm) thicknesses found in the TEM images. The carbonization process broke down the structure of the PDA film, which causes the layer to become thinner. As a result, the mean hydrodynamic size of the AlTi-MgO@C NPs was reduced to 60 nm.

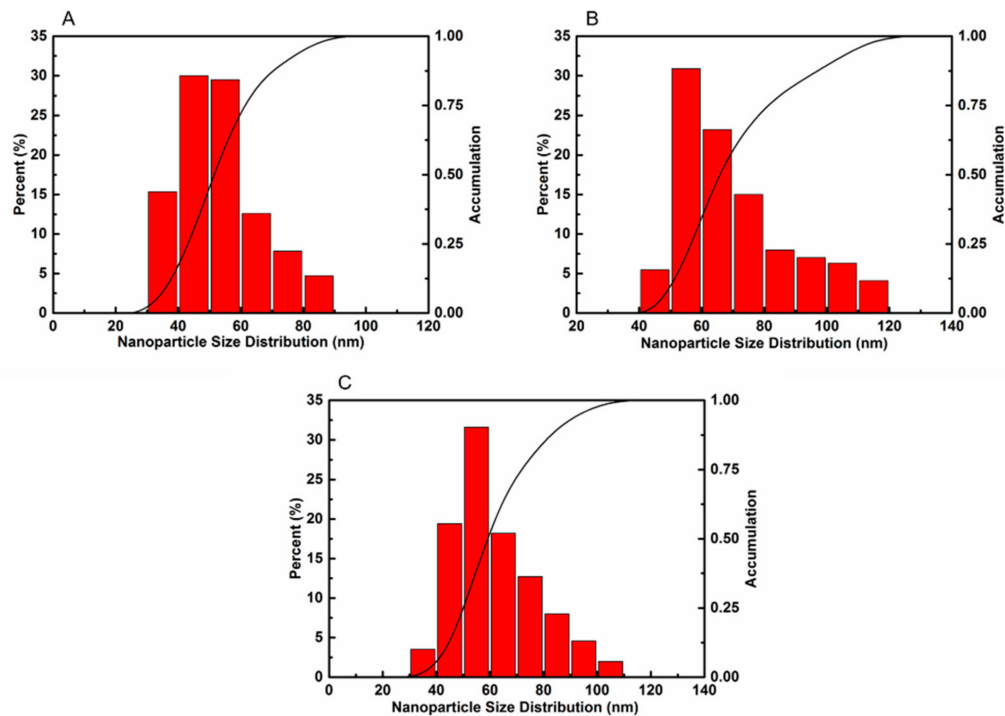


**Figure 6.** Hydrodynamic sizes of: (A) AlTi-MgO NPs; (B) AlTi-MgO@PDA NPs; and (C) AlTi-MgO@C NPs in the aqueous solution.

### 3.2. Surface Treatment and Physical Properties of the NPs in Steel

Dai et al. reported that polydopamine can act as a template for functionalizing a coated material surface and will form a carbon structure after subsequent heat treatment [15]. The carbonized NPs were found to exist in a stable form in an appropriate solvent, exhibiting good monodispersity and reduction in the aggregation of the NPs [15,22,23]. In the subsequent process of high-temperature steelmaking, the insignificant amount of carbon found in the coating of the surface-treated NPs exhibited little or no pollution in the molten steel [24].

The NPs could be regarded as the heterogenous nuclei that inhibits the movement of the grain boundary. Furthermore, the dispersive and fine inclusions can induce intragranular acicular ferrite. Both these processes can be used to improve the properties of materials. However, NPs can easily become agglomerated due to the effect of size and intense Brownian motion collisions. This agglomeration in the molten steel was closely linked to the wettability of the NPs in the molten steel and thus, can significantly affect the utilization ratio of the NPs in the steel.

After the NPs were added to the molten steel, they passed through the air–steel interface and were stirred by the Ar gas flow and by the force exerted by the furnace. After the NPs entered the liquid steel, they evolved into nucleating agents and denaturants of the inclusions in the steelmaking process. The agglomerating nature of the NPs has a significant influence on the distribution and characteristics of the inclusions in the steel. In the simulation of inclusions in a metallurgic reactor, the Stokes formula typically considers the kinematic viscosity, the equivalent radius of the inclusions and the difference in the density of the fluid and the inclusion. Furthermore, Wang [25] assumed that in liquid steel, NPs with a particle size of 50 nm floated up by only about 100 nm in 60 min and thus, the movement of NPs in the vertical direction can be ignored. Therefore, we can conclude that the NPs immersed into

the molten steel will not float to the air–steel interface. The wettability of the NP in high-temperature molten steel is an important factor affecting its utilization ratio in liquid steel. The wetting energy is typically used to assess the wettability of an NP in liquid steel, which can be calculated as follows:

$$W_i = \gamma_{LG} \times \cos \theta, \quad (1)$$

where  $W_i$  is the wetting work of the  $i$ th NP;  $\gamma_{LG}$  is the surface tension of the liquid steel; and  $\theta$  is the contact angle, which is shown in the diagram in Figure 7. Equation (1) demonstrates that the wettability of the NPs in the molten steel is determined by the contact angle ( $\theta$ ) as minimizing the contact angle improves the wettability. A contact angle that is greater than  $90^\circ$  indicates that the NPs are not wetted with the molten steel as the resulting strong hydrophobic effect would cause the NPs to strongly repel the surrounding medium.

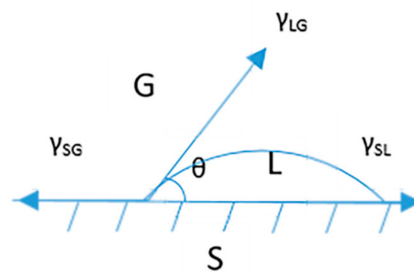


**Figure 7.** Contact angle diagram, showing the gas (G), liquid (L) and solid (S) regions, with definitions of the contact angle ( $\theta$ ) and the solid–gas ( $\gamma_{SG}$ ), liquid–gas ( $\gamma_{LG}$ ) and solid–liquid ( $\gamma_{SL}$ ) surface tensions.

Depending on the type of inclusions present in the steel, it is assumed that the added NPs will form corresponding oxides after they react with the dissolved oxygen in the molten steel. The contact angles of  $\text{Al}_2\text{O}_3$ , MgO and pyrographite with liquid steel were found to be  $100\text{--}141^\circ$  [26],  $130^\circ$  [27] and  $50^\circ$  [28], respectively, under a helium gas environment. This signifies that the contact angle of the AlTi-MgO@C NPs coated with a carbon layer is much lower than that of the AlTi-MgO NPs. Thus, the AlTi-MgO@C NPs possess superior wettability in the high-temperature molten steel and a greater number of effective particles will enter into the molten steel, creating an increased NP utilization ratio. Although the contact angle of these AlTi-MgO@C NPs have been shown in theory, more experimental evidence is needed to prove the wettability of these AlTi-MgO@C NPs in the molten steel.

#### 4. Conclusions

1. The AlTi-MgO alloy NPs were selected as the pre-dispersed medium in this study, with the average AlTi-MgO NPs size being 50 nm after pre-dispersion. A new type of core-shell structure that was comprised of AlTi-MgO@C NPs was successfully synthesized by dopamine self-polymerization under alkaline conditions and a high-temperature carbonization process, which can be used for steelmaking.
2. After the surface treatment, the size and composition of the NPs exhibited good dispersion of the NPs in the aqueous solution, with the width of the shell layer being about 10 nm. After immersion in hot HCl acid for several hours, the NP coating contained only amorphous and graphitic carbon, which was confirmed by XRD pattern analysis and the high-resolution TEM images of the surface-treated NPs. These results confirmed the presence of a carbon layer on the surface of the treated NPs.
3. Due to the different compositions of the NP coatings, the theoretical results show that after the surface treatment, the AlTi-MgO NPs have a smaller contact angle in the high-temperature liquid steel compared to the original AlTi-MgO NPs coated with PDA, indicating the superior

wettability of the AlTi-MgO@C NPs. Furthermore, this suggests that surface treatment will greatly increase the NP utilization ratio.

**Author Contributions:** Jinglong Qu conceived and designed the experiments and interpreted the data; Shufeng Yang and Jingshe Li wrote the paper; Shufeng Yang and Hao Guo analyzed the data and collected the literatures; Hao Guo and Tiantian Wang performed the experiments.

**Acknowledgments:** This research is supported by the National Science Foundation of China (No. 51574190).

**Conflicts of Interest:** The authors declare no conflict of interest.

## References

1. Gelde, L.; Cuevas, A.L.; Martínez de Yuso, M.V.; Benavente, J.; Vega, V.; González, A.S.; Prida, V.M.; Hernando, B. Influence of TiO<sub>2</sub>-coating layer on nanoporous alumina membranes by ALD technique. *Coatings* **2018**, *8*, 60. [[CrossRef](#)]
2. Vázquez Martínez, J.M.; Salguero Gómez, J.; Batista Ponce, M.; Botana Pedemonte, F.J. Effects of laser processing parameters on texturized layer development and surface features of Ti<sub>6</sub>Al<sub>4</sub>V alloy samples. *Coatings* **2017**, *8*, 6. [[CrossRef](#)]
3. Murugan, P.; Krishnamurthy, M.; Jaisankar, S.N.; Samanta, D.; Baran Mandal, A. Controlled decoration of the surface with macromolecules: Polymerization on a self-assembled monolayer (SAM). *Chem. Soc. Rev.* **2015**, *44*, 3212–3243. [[CrossRef](#)] [[PubMed](#)]
4. Jiang, J.H.; Zhu, L.P.; Zhu, L.J.; Zhu, B.K.; Xu, Y.Y. Surface characteristics of a self-polymerized dopamine coating deposited on hydrophobic polymer films. *Langmuir* **2011**, *27*, 14180–14187. [[CrossRef](#)] [[PubMed](#)]
5. Wei, Q.; Zhang, F.L.; Li, J.; Li, B.J.; Zhao, C.S. Oxidant-induced dopamine polymerization for multifunctional coatings. *Polym. Chem.* **2010**, *1*, 1430–1433. [[CrossRef](#)]
6. Ball, V.; Del Frari, D.; Michel, M.; Buehler, M.J.; Toniazzo, V.; Singh, M.K.; Gracio, J.; Ruch, D. Deposition mechanism and properties of thin polydopamine films for high added value applications in surface science at the nanoscale. *BioNanoScience* **2012**, *2*, 16–34. [[CrossRef](#)]
7. Wang, S.B.; Min, Y.L.; Yu, S.H. Synthesis and magnetic properties of uniform hematite nanocubes. *J. Phys. Chem. C* **2007**, *111*, 3551–3554. [[CrossRef](#)]
8. Yu, X.L.; Deng, J.J.; Zhan, C.Z.; Lv, R.; Huang, Z.H.; Kang, F.Y. A high-power lithium-ion hybrid electrochemical capacitor based on citrate-derived electrodes. *Electrochim. Acta* **2017**, *228*, 76–81. [[CrossRef](#)]
9. Lei, C.; Han, F.; Li, D.; Li, W.C.; Sun, Q.; Zhang, X.Q.; Lu, A.H. Dopamine as the coating agent and carbon precursor for the fabrication of N-doped carbon coated Fe<sub>3</sub>O<sub>4</sub> composites as superior lithium ion anodes. *Nanoscale* **2013**, *5*, 1168–1175. [[CrossRef](#)] [[PubMed](#)]
10. Yue, Q.; Wang, M.H.; Sun, Z.K.; Wang, C.; Wang, C.; Deng, Y.H.; Zhao, D.Y. A versatile ethanol-mediated polymerization of dopamine for efficient surface modification and the construction of functional core-shell nanostructures. *J. Mater. Chem. B* **2013**, *1*, 6085–6093. [[CrossRef](#)]
11. Liu, Y.L.; Ai, K.L.; Lu, L.H. Polydopamine and its derivative materials: Synthesis and promising applications in energy, environmental, and biomedical fields. *Chem. Rev.* **2014**, *114*, 5057–5115. [[CrossRef](#)] [[PubMed](#)]
12. Kasemset, S.; Lee, A.; Miller, D.J.; Freeman, B.D.; Sharma, M.M. Effect of polydopamine deposition conditions on fouling resistance, physical properties, and permeation properties of reverse osmosis membranes in oil/water separation. *J. Membr. Sci.* **2013**, *425*, 208–216. [[CrossRef](#)]
13. Lee, H.; Dellatore, S.M.; Miller, W.M.; Messersmith, P.B. Mussel-inspired surface chemistry for multifunctional coatings. *Science* **2007**, *31*, 426–430. [[CrossRef](#)] [[PubMed](#)]
14. Kang, S.M.; You, I.; Cho, W.K.; Shon, H.K.; Lee, T.G.; Choi, I.S.; Karp, J.M.; Lee, H. One-step modification of superhydrophobic surfaces by a mussel-inspired polymer coating. *Angew. Chem. Int. Ed.* **2010**, *49*, 9401–9404. [[CrossRef](#)] [[PubMed](#)]
15. Liu, R.; Mahurin, S.M.; Li, C.; Unocic, R.R.; Idrobo, J.C.; Gao, H.J.; Pennycook, S.J.; Dai, S. Dopamine as a carbon source: The controlled synthesis of hollow carbon spheres and yolk-structured carbon nanocomposites. *Angew. Chem. Int. Ed.* **2011**, *50*, 6799–6802. [[CrossRef](#)] [[PubMed](#)]
16. Gao, X.Z.; Yang, S.F.; Li, J.S.; Yang, Y.D.; Chattopadhyay, K. Inclusion characteristics and microstructure properties under different cooling conditions in steel with nanoparticles addition. *Ironmak. Steelmak.* **2017**, 1–7. [[CrossRef](#)]

17. Zener, C. Private Communication to CS Smith. *Trans. Am. Inst. Metall. Eng.* **1949**, *175*, 15–17.
18. Gao, X.Z.; Yang, S.F.; Li, J.S.; Liao, H.; Gao, W.; Wu, T. Addition of MgO nanoparticles to carbon structural steel and the effect on inclusion characteristics and microstructure. *Metall. Mater. Trans. B* **2016**, *47*, 1124–1136. [[CrossRef](#)]
19. Gao, X.Z.; Yang, S.F.; Li, J.S.; Yang, Y.D.; Chattopadhyay, K.; Mclean, A. Effects of MgO nanoparticle additions on the structure and mechanical properties of continuously cast steel billets. *Metall. Mater. Trans. A* **2016**, *47*, 461–470. [[CrossRef](#)]
20. Gao, X.Z.; Yang, S.F.; Li, J.S.; Ma, A.; Chattopadhyay, K. Improvement of utilization ratio of nanoparticles in steel and its influence on acicular ferrite formation. *Steel Res. Int.* **2017**, *88*. [[CrossRef](#)]
21. Gong, W.; Chen, W.S.; He, J.P.; Tong, Y.; Liu, C.; Su, L.; Gao, B.; Yang, H.K.; Zhang, Y.; Zhang, X.J. Substrate-independent and large-area synthesis of carbon nanotube thin films using ZnO nanorods as template and dopamine as carbon precursor. *Carbon* **2015**, *83*, 275–281. [[CrossRef](#)]
22. Liang, Y.R.; Liu, H.; Li, Z.H.; Fu, R.W.; Wu, D.C. In situ polydopamine coating-directed synthesis of nitrogen-doped ordered nanoporous carbons with superior performance in supercapacitors. *J. Mater. Chem. A* **2013**, *1*, 15207–15211. [[CrossRef](#)]
23. Kong, J.H.; Yee, W.A.; Wei, Y.F.; Yang, L.P.; Anq, J.M.; Phua, S.L.; Wong, S.Y.; Zhou, R.; Dong, Y.L.; Li, X.; et al. Silicon nanoparticles encapsulated in hollow graphitized carbon nanofibers for lithium ion battery anodes. *Nanoscale* **2013**, *5*, 2967–2973. [[CrossRef](#)] [[PubMed](#)]
24. Mu, W.Z.; Mao, H.H.; Jönsson, P.G.; Nakajima, K.J. Effect of carbon content on the potency of the intragranular ferrite formation. *Steel Res. Int.* **2016**, *87*, 311–319. [[CrossRef](#)]
25. Wang, G.C.; Wang, T.M.; Li, S.N.; Fang, K.M. Study on the process of adding Al<sub>2</sub>O<sub>3</sub> nano-powder to molten pure iron. *Chin. J. Eng.* **2007**, *29*, 578–581. (In Chinese)
26. Zhao, L.Y.; Sahajwalla, V. Interfacial phenomena during wetting of graphite/alumina mixtures by liquid iron. *ISIJ Int.* **2003**, *43*, 1–6. [[CrossRef](#)]
27. Humenik, M.; Kingery, W.D. Metal-ceramic interactions: III, surface tension and wettability of metal-ceramic systems. *J. Am. Ceram. Soc.* **1954**, *37*, 18–23. [[CrossRef](#)]
28. Kostikov, V.I.; Maurakh, M.A.; Nozhkina, A.V. Wetting of diamond and graphite by liquid iron-titanium alloys. *Powder Metall. Met. Ceram.* **1971**, *10*, 62–64. [[CrossRef](#)]



© 2018 by the authors. Licensee MDPI, Basel, Switzerland. This article is an open access article distributed under the terms and conditions of the Creative Commons Attribution (CC BY) license (<http://creativecommons.org/licenses/by/4.0/>).